SAS 6180 ARTICLE IN PRESS No. of Pages 20, Model 3+
18 January 2008 Disk Used

Available online at www.sciencedirect.com
ScienceDirect
International Journal of Solids and Structures xxx (2008) xxx–xxx
INTERNATIONAL JOURNAL OF SOLIDS AND STRUCTURES
www.elsevier.com/locate/ijsolstr

Viscoplastic approach for rate-dependent failure analysis of concrete joints and interfaces

R. Lorefice [a], G. Etse [b,*], I. Carol [c]

[a] Universidad Nacional de Santiago del Estero, Argentina
[b] Universidad de Buenos Aires, Argentina – CONICET, Munecas 730, 10 A, 4000 Tucuman, Tucuman, Argentina
[c] ETSECCPB-UPC, Barcelona, Spain

Received 9 January 2007; received in revised form 25 November 2007

Abstract

In this work, a new rate-dependent interface model for computational analysis of quasi-brittle materials like concrete is presented. The model is formulated on the basis of the inviscid elastoplastic model by [Carol, I., Prat, P.C., López, C.M., 1997. "A normal/shear cracking model. Interface implementation for discrete analysis". Journal of Engineering Mechanics, ASCE, 123 (8), pp. 765–773.]. The rate-dependent extension follows the continuous form of the classical viscoplastic theory by [Perzyna, P., 1966. "Fundamental problems in viscoplasticity". Advances in Applied Mechanics, 9, pp. 244–368.]. According to [Ponthot, J.P., 1995. "Radial return extensions for viscoplasticity and lubricated friction". In: Proceedings of International Conference on Structural Mechanics and Reactor Technology SMIRT-13, Porto Alegre, Brazil, (2), pp. 711–722.] and [Etse, G., Carosio, A., 2002. "Diffuse and localized failure predictions of Perzyna viscoplastic models for cohesive-frictional materials". Latin American Applied Research (32), pp. 21–31.] it includes a consistency parameter and a generalized yield condition for the viscoplastic range that allows an straightforward extension of the full backward Euler method for viscoplastic materials. This approach improves the accuracy and stability of the numerical solution. The model predictions are tested against experimental results on mortar and concrete specimens that cover different stress paths at different strain rates. The results in this work demonstrate, on one hand, the capabilities of the proposed elasto–viscoplastic interface constitutive formulation to predict the rate-dependency of mortar and concrete failure behavior, and, on the other hand, the efficiency of the numerical algorithms developed for the computational implementation of the model that include the consistent tangent operator to improve the convergence rate at the finite element level.

Keywords: Concrete; Failure; Interface; Rate-dependency; Viscoplasticity

1. Introduction

It is known that quasi-brittle materials like concrete present a highly complex mechanical behavior characterized by a strongly stress-state dependent failure response. The main and fundamental reason is the intrinsic

* Corresponding author. Tel./fax: +54 381 4226151.
E-mail addresses: lorefice@unse.edu.ar (R. Lorefice), getse@herrera.unt.edu.ar (G. Etse), Ignacio.Carol@upc.edu (I. Carol).

0020-7683/$ - see front matter © 2007 Elsevier Ltd. All rights reserved.
doi:10.1016/j.ijsolstr.2007.12.016

Please cite this article in press as: Lorefice, R. et al., Viscoplastic approach for rate-dependent failure analysis ..., Int. J. Solids Struct. (2008), doi:10.1016/j.ijsolstr.2007.12.016

heterogeneity due to the composite nature of its mesostructure. Presently, the influence of the concrete heterogeneity in its response behavior is concentrating significant attention of the international scientific community.

In this sense, most of the recent attempts focus on the development and use of discrete models instead of those based on continuum approaches, see a.o. Stankowski (1990), Vonk (1992), Carol et al. (1997), López Garello (1999), Vervuurt (1997), Slowik and Leite (2000), Chang et al. (2002a,b), Shi et al. (1999), Wang and Bittencourt (2001), among others. The increasing use of discontinuous models is mainly due to their mesh objective numerical predictions but also to the fact that they can be used in computational analysis at both meso and micro-mechanical levels.

Another relevant difficulty of the concrete mechanical behavior arises from its rheologic feature that is responsible for the significant time-effect dependence of its failure response. Essentially, two types of time-effects can be distinguished in concrete behavior. On the one hand, the time-dependent effect that appears during sustained load and/or deformation processes in concrete such as creep and relaxation. This type of time-effect is not taken into account in the present paper. On the other hand, the time-rate effect or, simply, the rate-dependent effect that controls the concrete fracture/cracking process evolution (phenomenon related to the activated energy that is necessary for the rupture of interatomics bounds). The rate dependence of concrete is activated during seismic loads, impacts and/or machine vibrations that act in most of the existing concrete structures and foundations. Contributions related to the experimental evidence of the rate-dependent effect are due to Watstein (1953), Takeda and Tachikawa (1962, 1971), Cowell (1966), Birkimer (1968), Birkimer and Lindemann (1971), Hughes and Gregory (1972), Hughes and Watson (1978), Reinhardt (1982, 1984, 1985), Ross et al. (1989), Ross (1991), Ross et al. (1995), Ross et al. (1996), John and Shah (1987), John et al. (1992), Tedesco et al. (1989, 1991, 1993, 1997), Suaris and Shah (1984, 1985), Bresler and Bertero (1975), Dilger et al. (1978), Malvern et al. (1985), Bažant and Gettu (1992), Bažant et al. (1993, 1995) among others. The range of the evaluated strain rates was generally controlled by the type of loading devices used in each experimental research. For instance, Bresler and Bertero (1975) and Takeda and Tachikawa (1962) used hydraulic testing machines to load specimens at strain rates up to 1 s^{-1}. Hughes and Gregory (1972), Watstein (1953) and Hughes and Watson (1978) used a drop-weight impactor to achieve strain rates up to 10 s^{-1}. Ross et al. (1989, 1996) and Malvern et al. (1985) used a split Hopkinson Pressure Bar (SHPB) and obtained deformation rates between 10 and 10^3 s^{-1}. The strain at maximum strength or peak stress is an important parameter in the characterization of material behavior. There have been differing interpretations regarding how this strain varies with the strain rate. Watstein (1953) and Takeda and Tachikawa (1962) reported that the strain at peak stress increases with increasing strain rate. Contrarily, Hatano and Tsutsumi (1960) and Cowell (1966) found that it essentially remains constant while Hughes and Watson (1978), Dilger et al. (1978), and Dhir and Sangha (1972) have indicated that it decreases with increasing strain rate.

The contradictory findings can be partly attributed to the inconsistency in the loading methods used for the tests. However, and despite the differences in the authors findings regarding the variation of the strain at peak stress with the strain rate, they all demonstrated that the higher the strain rate, the more relevant the concrete rate dependence.

The strain rate dependence of the concrete compressive and tensile peak stresses is typically illustrated by means of the dynamic increase factor curve DIF that shows the variation of the dynamic to static uniaxial strengths with the applied strain rates on a semi-log or log–log scale. Fig. 1 shows different DIF curves obtained by several authors. They are compared with the CEB–DIF curves for 30 and 70 MPa concrete strengths. One important aspect of all the experimental data in Fig. 1 independently of the particular test device and procedure considered, is that above the strain rate of 1 sec^{-1} they all show the same trend, i.e., a stronger increment of the DIF. The data from Birkimer (1968), and Birkimer and Lindemann (1971) were obtained by measuring the strain pulses on long concrete rods impacted by metallic projectiles. McVay (1988) and Antoun (1991) obtained their data by back calculating stress and strain from spall tests. Data collected by Ross et al. (1989, 1996) were obtained using two different size split Hopkinson pressure bars, three different specimen sizes, and six different concrete mixtures. Moreover, they performed two different type of tensile tests, the direct tensile test and the splitting tensile test (Brazilian test). Finally, data by John et al. (1992) were obtained from independent SHPB tests. As indicated before, in all cases, and for strain rates larger than 1 s^{-1},

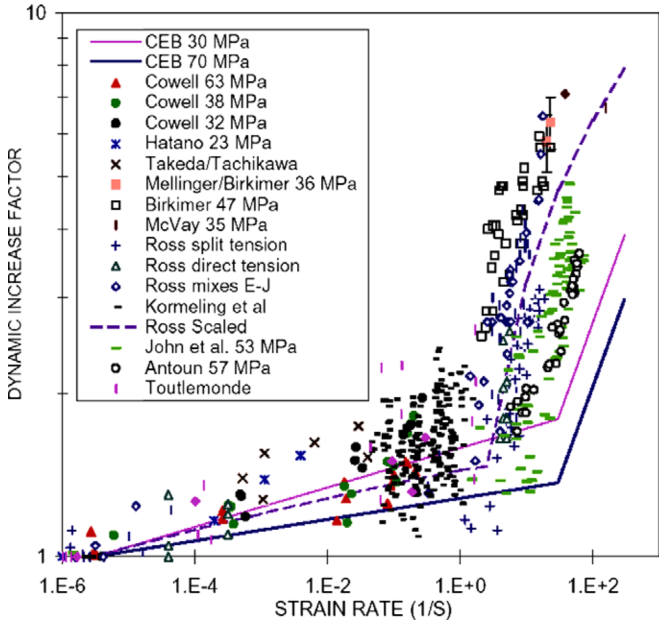

Fig. 1. Experimental test data – pure tension test.

very high dynamic tensile strengths were observed when compared to the quasi-static strength of concrete. Regarding the influence of the concrete static compressive strength in its strain rate sensitivity, the experimental results of Cowell (1966) as well as Kormeling et al. (1980) demonstrate that concretes with the lower compressive strength exhibited the higher DIF in tension.

The experimental evidence shows also that concrete rate dependency is higher in tension than in compression. Particularly, in the tension regime we can distinguish between a low to moderate rate-dependency range for strain rates from 10^{-6} to 1.0 s^{-1}, on the one hand, and a high rate-dependency range for strain rates greater than 1.0 s^{-1}, on the other hand. The strong change of the DIF that takes place at this upper limit of strain rate (1.0 s^{-1}) can be observed in Fig. 1. In the low to moderate regime, moisture content plays an important role in concrete over-strength, Rossi et al. (1992), Rossi (1997), Cadoni et al. (2001a,b), Ross et al. (1996). The free water in the micro-pores originate the so-called Stefan-effect (Rossi, 1997) causing a strengthening effect in concrete with increasing loading rate. This Stefan-effect is the phenomenon that occurs when a viscous liquid is trapped between two plates that are rapidly separated, causing a reaction force on the plates that is proportional to the velocity of separation. In Cadoni et al. (2001a,b), a different explanation for the influence of the moisture content is given, based on the principle of wave propagation in concrete. When a pore is not filled with water, it will locally reflect the incoming stress wave. The multiple reflections of all pores together may cause a considerable stress increase giving rise to material damage. When a stress wave meets a pore that is filled with liquid the reflected stress is not big enough to cause the stress increase. Therefore, wet concrete exhibits less damage and more pronounced rate-dependent effects than dry concrete when subjected to stress waves. This interpretation by Cadoni et al. (2001a,b) provides an explanation to the strength differences between wet and dry concrete. However, it fails to explain the increase in strength that occurs in concrete under dynamic loading. Actually, the rate dependency in the high loading rate regime is mainly due to micro-inertia effects in the fracture process zone, Weerheijm et al. (2001, 2003), Brara and Klepaczko (2006). This mechanism is completely different to the one that governs the rate-dependency in the low to moderate strain rate regime.

Conceptual and numerical standpoint studies regarding the influence of the strain-rate in concrete and cementitious materials at macromechanic level are a.o. due to Etse and Carosio (2002), Bažant et al. (2000), Burlion et al. (2000), Winnicki et al. (2001), Grote et al. (2001) and Park et al. (2001). At the mesomechanic level, the authors that evaluated the concrete strain rate sensitivity are a.o., Ruiz et al. (2000), Xu and

Please cite this article in press as: Lorefice, R. et al., Viscoplastic approach for rate-dependent failure analysis ..., Int. J. Solids Struct. (2008), doi:10.1016/j.ijsolstr.2007.12.016

Needleman (1994), Tvergaard and Hutchinson (1993), Sluys and Liu (2003), Bažant and Li (1997), Bažant and Oh (1982), and Li and Bažant (1997). Bažant et al. (2000) proposed a rate-dependent extended version of the Microplane M4 model by means of a viscoelastic Maxwell chain. Etse and Carosio (2002) as well as Winnicki et al. (2001) worked on a rate-dependent extension of elasto-plastic models for concrete using Perzyna's visco-plasticity theory in order to include the strain rate and time effects in the material response. Etse and Carosio (2002) considered the continuous Perzyna viscoplasticity concept by Ponthot (1995) to evaluate the localized failure indicator performance. Winnicki et al. (2001) extended the Hoffman model for concrete by introducing the consistent viscoplasticity concept by Wang (1997), see also Wang and Sluys (2000).

In this work, a new viscoplastic-based time/rate-dependent interface model for quasi-brittle materials like concrete is presented. Discussion focusses on the model performance to capture rate effects on failure behavior of cementitious-like materials. Based on the previously discussed experimental evidence regarding the different mechanisms controlling the concrete rate dependency in the low to moderate and the high strain rate regimes, and as the proposed model takes into account the rate dependency by means of the viscoplastic theory, the numerical predictions in this work are restricted to the low to moderate regime of strain rates. The interface elasto–viscoplastic formulation is based on a continuum Perzyna-type extension of the inviscid interface model by Carol et al. (1997). Contrarily to the classical Perzyna formulation this continuum theory by Ponthot (1995) includes a generalized consistency condition for the viscoplastic range which allows the extension of the well-known numerical methods of classical plasticity to rate-dependent models. After formulating the constitutive equations of the viscoplastic interface model the numerical algorithms developed for the computational implementation of the model are presented, including the consistent tangent operator to improve the convergence rate at the finite element level.

In order to properly calibrate the model, the experimental tests on concrete specimens at different strain rates by Suaris and Shah (1984, 1985) are considered. The numerical analysis of concrete and mortar dynamic behaviors under different stress paths in this work demonstrate, on the one hand, the efficiency of the developed numerical tools and, on the other hand, the capabilities of the proposed formulation to reproduce the strength and ductility dependency of quasi-brittle materials like mortar and concrete on the considered strain rates.

2. Continuous Perzyna rate-dependent formulation

Similar to the flow theory of plasticity, the elasto–viscoplastic constitutive relations by Perzyna (1966) may be written as

$$\dot{\boldsymbol{\sigma}} = \dot{\boldsymbol{\sigma}}_e - \dot{\boldsymbol{\sigma}}_{vp} = \mathcal{E} : (\dot{\boldsymbol{\varepsilon}} - \dot{\boldsymbol{\varepsilon}}_{vp}) \tag{1}$$

$$\dot{\boldsymbol{\varepsilon}}_{vp} = \boldsymbol{g}(\psi, F, \boldsymbol{\sigma}) = \frac{1}{\eta}\langle\psi(F)\rangle\boldsymbol{m} \tag{2}$$

$$\boldsymbol{m} = \mathcal{A}^{-1} : \boldsymbol{n} = \mathcal{A}^{-1} : \frac{\partial F}{\partial \boldsymbol{\sigma}} \tag{3}$$

$$\psi(F) = \left[\frac{F(\boldsymbol{\sigma}, \boldsymbol{q})}{F_o}\right]^N \tag{4}$$

$$\dot{\boldsymbol{q}} = \frac{1}{\eta}\langle\psi(F)\rangle\mathcal{H} : \boldsymbol{m} \tag{5}$$

where $\dot{\boldsymbol{\varepsilon}}_{vp}$ represents the viscoplastic portion of the total strain rate tensor $\dot{\boldsymbol{\varepsilon}}$, η the fluidity parameter (apparent viscosity) and $\dot{\boldsymbol{q}}$ the rate of hardening/softening variables defined as a tensor of arbitrary order. Eq. (1) follows from the additive decomposition of the total strain rate into an elastic and a viscoplastic part $\dot{\boldsymbol{\varepsilon}} = \dot{\boldsymbol{\varepsilon}}_e + \dot{\boldsymbol{\varepsilon}}_{vp}$, quite similar to the Prandtl–Reuss equations in case of inviscid elasto-plastic constitutive materials. Thereby $\mathcal{E}$ is the fourth order elastic tensor. Eqs. (2) and (3) describe a general non-associated flow rule that controls the direction of the viscoplastic strains. This is defined by the gradient tensor $\boldsymbol{m}$ obtained by a modification of the gradient tensor $\boldsymbol{n}$ to the yield surface F by means of the fourth order transformation tensor $\mathcal{A}$. $\psi(F)$ in Eq. (4) is a dimensionless monotonically increasing over-stress function that depends on the inviscid yield function $F(\boldsymbol{\sigma}, \boldsymbol{q})$ which defines the limit of the elastic domain. F_o represents a normalizing factor, usually chosen equal to the initial yield limit. N is a parameter that should satisfy $N \geqslant 1$ and defines the order of the Perzyna's viscoplasticity while the Mc Cauley brackets in Eq. (2) and (5) states the features of the over-stress function as

$$\langle \psi(F) \rangle = \begin{cases} \psi(F) & \text{if} \quad F > 0 \\ 0 & \text{if} \quad F \leqslant 0 \end{cases} \tag{6}$$

Finally, Eq. (5) represents the evolution law of the hardening/softening variables $\boldsymbol{q}$ by means of a suitable tensorial function $\mathcal{H}$ of the state variables.

In the continuous Perzyna formulation, see Ponthot (1995), Eqs. (1)–(5) are complemented by the consistency viscoplastic parameter $\dot{\lambda}$ which is defined in terms of the over-stress function,

$$\dot{\lambda} = \frac{1}{\eta} \langle \psi(F) \rangle \tag{7}$$

So that the evolution Eqs. (2) and (5) take now the classical forms

$$\dot{\boldsymbol{\varepsilon}}_{vp} = \dot{\lambda} \boldsymbol{m} \tag{8}$$

$$\dot{\boldsymbol{q}} = \dot{\lambda} \mathcal{H} : \boldsymbol{m} = \dot{\lambda} \boldsymbol{h} \tag{9}$$

being $\boldsymbol{h} = \mathcal{H} : \boldsymbol{m}$. In the particular case of one state variable, Eq. (9) turns into

$$\dot{q} = \dot{\lambda} h \tag{10}$$

with h a scalar function of $\boldsymbol{m}$. In what follows this case will be considered and the extension to the case of several state variables is straightforward. After eliminating $\dot{\lambda}$ between (7) and (8) and applying the inverse function ψ^{-1} in both terms follows

$$F = \psi^{-1} \left(\frac{\| \dot{\boldsymbol{\varepsilon}}_{vp} \|}{\| \boldsymbol{m} \|} \eta \right) = \psi^{-1}(\dot{\lambda} \eta) \tag{11}$$

We may now define the new constrain condition for the viscoplastic range restating (11) as

$$\overline{F} = F - \psi^{-1}(\dot{\lambda} \eta) = 0 \tag{12}$$

which represents a generalization of the inviscid yield condition $F = 0$ for rate-dependent Perzyna viscoplastic materials. The name *continuous formulation* is due to the fact that the condition $\eta = 0$ (no viscosity effect) leads to the elastoplastic yield condition $F = 0$, see Etse and Carosio (2002). Moreover, from (7) follows that when $\eta \to 0$ the consistency parameter remains finite and positive since also the over-stress goes to zero. The other extreme case, $\eta \to \infty$, leads to the inequality $\overline{F} < 0$ for every possible stress state, indicating that only elastic response may be activated.

The constrain defined by Eq. (12) allows a generalization of the Kuhn–Tucker conditions

$$\dot{\lambda} \overline{F} = 0, \quad \dot{\lambda} \geqslant 0, \quad \overline{F} \leqslant 0. \tag{13}$$

Finally, the generalized consistency condition for the viscoplastic range expands into

$$\dot{\overline{F}} = \boldsymbol{n} : \dot{\boldsymbol{\sigma}} + \bar{r} \dot{q} + \bar{s} \ddot{\lambda} = 0 \tag{14}$$

where

$$\bar{r} = \frac{\partial \overline{F}}{\partial q} = \left(\frac{\partial F}{\partial q} - \frac{\partial \psi^{-N}(\dot{\lambda} \eta)}{\partial q} \right) \tag{15}$$

and

$$\bar{s} = -\frac{\partial \varphi^{-N}(\eta \dot{\lambda})}{\partial \dot{\lambda}} \tag{16}$$

The constrain in Eq. (12) and, particularly, the generalized consistency condition (14) play an important role in the numerical integration of continuous Perzyna constitutive models. In this regard, linearization of Eq. (14) allows, on the one hand, the application of the well-known Backward-Euler or Closest Point Projection method of inviscid elastoplasticity to obtain full implicit stress integration procedures during Perzyna-type viscoplastic processes. On the other hand, it allows the formulation of the algorithmic tangent operator to improve the convergence rate at the finite element level in the framework of the Newton-Raphson method. Consequently, continuous Perzyna model formulations are related to a superior efficiency of the numerical procedures for stress integration as compared to classical Perzyna viscoplasticity.

Other interesting modification to the classical Perzyna formulation is due to Wang (1997), which includes the strain rate as an additional state variable into the flow and viscoplastic potential functions, *i.e.,*

$$F^{vp} = F^{vp}(\boldsymbol{\sigma}, \boldsymbol{q}, \dot{\boldsymbol{\varepsilon}}) \tag{17}$$

This also leads to the formulation of the rate-dependent Kuhn–Tucker conditions for the viscoplastic range similarly to the continuous Perzyna formulation.

3. Time-dependent interface model formulation

In this section, the rate-dependent extension of the interface model by Carol et al. (1997) is presented. The viscoplastic yield condition of the interface constitutive model is defined as

$$\overline{F} = F - \psi^{-1}(\dot{\lambda}\eta) = \tau^2 - (c - \sigma \tan\phi)^2 + (c - \chi \tan\phi)^2 - (\dot{\lambda}\eta) \tag{18}$$

where a Perzyna exponent $N = 1$ is considered. The interface behavior is formulated in terms of the stress vector $\mathbf{t} = [\sigma, \tau]^T$, with normal and tangential stress components to the interface plane, and corresponding relative displacements $\mathbf{u} = [u, v]^T$. The tensile strength χ (vertex of hyperbola), the shear strength c (cohesion strength) and the internal friction angle ϕ are model parameters, while $\dot{\lambda}$ is the viscoplastic multiplier defined as in Eq. (7) being η the viscosity. In Eq. (18), two limit situations can be distinguished: (a) cracking under pure tension, with zero shear stress (Mode I), when the yield surface is reached along the horizontal axis, and (b) cracking under shear and very high compression, when the yield surface is reached in its asymptotic region, where the hyperbola approaches a Mohr-Coulomb criterion, which is called "asymptotic Mode II". The hyperbolic criteria provides a smooth transition between these two limit states. The evolution of the rate-dependent fracture process is driven by the cracking parameters χ and c, which depends on a single state variable: the work spent during viscoplastic crack formation, q^{vcr}. As q^{vcr} increases, c and χ are assumed to linearly decrease from their initial values χ_0 and c_0 in terms of an intermediate scaling function S, defined as

$$\chi = \chi_0(1 - S(\xi_\chi)) \quad c = c_0(1 - S(\xi_c)) \tag{19}$$

with

$$S(\xi_\chi) = \frac{\mathrm{e}^{-\alpha_\chi}\xi_\chi}{1 + (\mathrm{e}^{-\alpha_\chi} - 1)\xi_\chi} \quad S(\xi_c) = \frac{\mathrm{e}^{-\alpha_c}\xi_c}{1 + (\mathrm{e}^{-\alpha_c} - 1)\xi_c} \tag{20}$$

where $\xi_\chi = q^{vcr}/G_f^I$, $\xi_c = q^{vcr}/G_f^{II}$ and α_χ, α_c are material parameters. Here, G_f^I and G_f^{II} are the fracture energies in Mode I and Mode II, respectively. As the friction angle is assumed to remain constant, the evolution law of q^{vcr} that defines the necessary amount of release energy to open a single crack in a time-dependent tensile or compressive fracture processes is

$$\dot{q}^{vcr} = \mathbf{t}^T\dot{\mathbf{u}}^{vcr} \tag{21}$$

and

$$\dot{\mathbf{u}}^{vcr} = \dot{\lambda}\mathbf{A}\mathbf{n} \tag{22}$$

the critical rate-dependent displacement vector at the interface. The viscoplastic flow is fully associated in tension while non-associated in compression. In the viscoplastic interface model formulation, Eq. (3) is expressed in matrix form as $\mathbf{m} = \mathbf{A}\mathbf{n}$, with

$$\mathbf{n} = \frac{\partial F}{\partial \mathbf{t}} = \left[\frac{\partial F}{\partial \sigma}, \frac{\partial F}{\partial \tau}\right]^T = [2\tan\phi(c - \sigma\tan\phi), 2\tau]^T \tag{23}$$

Thereby, the transformation matrix $\mathbf{A}$ defining the loss of normality of the rate-dependent crack opening displacement evolution vector $\dot{\mathbf{u}}^{vcr}$ in the viscoplastic interface model is obtained as

$$\mathbf{A} = \begin{cases} \begin{pmatrix} 1 & 0 \\ 0 & 1 \end{pmatrix} & \text{if} \quad \sigma \geqslant 0 \\ \begin{pmatrix} f_{\sigma^{dil}} f_{c^{dil}} & 0 \\ 0 & \left(1 - \left|\frac{\sigma\tan\phi}{\tau}\right|\right) \end{pmatrix} & \text{if} \quad \sigma < 0 \end{cases} \tag{24}$$

The factors $f_\sigma^{dil} = 1 - |\sigma|/\sigma^{dil}$ and $f_c^{dil} = 1 - c/c_0$ account for the dilatancy effects in the compressive regime by means of a reduction of the normal stress component to the interface, see Carol et al. (1997) and López Garello (1999). In the expression of f_σ^{dil}, σ^{dil} is a model parameter representing the value at which dilatancy vanishes.

The continuum viscoplastic formulation of the rate-dependent interface constitutive model is completed by the following equations

$$\dot{\mathbf{u}} = \dot{\mathbf{u}}^{el} + \dot{\mathbf{u}}^{vcr} \tag{25}$$

$$\dot{\mathbf{u}}^{el} = \mathbf{E}^{-1}\dot{\mathbf{t}} \tag{26}$$

$$\dot{\mathbf{t}} = \mathbf{E}(\dot{\mathbf{u}} - \dot{\mathbf{u}}^{vcr}) \tag{27}$$

where $\dot{\mathbf{u}}^T = (\dot{u}, \dot{v})$ is the rate of the relative displacement vector which is decomposed into the elastic or recoverable portion and the rate-dependent crack opening component, $\dot{\mathbf{u}}^{el}$ and $\dot{\mathbf{u}}^{vcr}$, respectively. $\mathbf{E}$ defines a fully uncoupled normal/tangential elastic stiffness at the interface

$$\mathbf{E} = \begin{pmatrix} E_N & 0 \\ 0 & E_T \end{pmatrix} \tag{28}$$

The viscoplastic consistency condition in Eq. (14) takes now the form $\dot{\overline{F}} = \mathbf{n}^T\dot{\mathbf{t}} + \bar{r}\dot{q}^{vcr} + \bar{s}\ddot{\lambda} = 0$, with $\bar{r}$ and $\bar{s}$ defined as

$$\bar{r} = \left(\frac{\partial F}{\partial c}\frac{\mathrm{d}c}{\mathrm{d}q^{vcr}} + \frac{\partial F}{\partial \chi}\frac{\mathrm{d}\chi}{\mathrm{d}q^{vcr}}\right) \tag{29}$$

$$\frac{\partial F}{\partial c} = 2\tan\phi(\sigma - \chi) \tag{30}$$

$$\frac{\partial F}{\partial \chi} = -2\tan\phi(c - \chi\tan\phi) \tag{31}$$

with

$$\frac{\mathrm{d}c}{\mathrm{d}q^{vcr}} = -\frac{c_0 \mathrm{e}^{-\alpha_c} G_f^{II}}{[(\mathrm{e}^{-\alpha_c} - 1)q^{vcr} + G_f^{II}]^2} \tag{32}$$

$$\frac{\mathrm{d}\chi}{\mathrm{d}q^{vcr}} = -\frac{\chi_0 \mathrm{e}^{-\alpha_\chi} G_f^{I}}{[(\mathrm{e}^{-\alpha_\chi} - 1)q^{vcr} + G_f^{I}]^2} \tag{33}$$

and

$$\bar{s} = -\frac{\partial\varphi^{-1}(\eta\dot{\lambda})}{\partial\dot{\lambda}} = -\eta \tag{34}$$

4. Stress integration procedure

In the context of the Closest Point Projection Method (CPPM), the viscoplastic crack opening displacement at time "n" takes the form, see Carosio et al. (2000)

$$\mathbf{u}_n^{vcr} = \mathbf{u}_{n-1}^{vcr} + \Delta\lambda_n \mathbf{A}_n \mathbf{n}_n \tag{35}$$

Ignoring the subscripts "n", the incremental form of stress and state variables can be expressed as

$$\Delta\mathbf{t} = \mathbf{E}(\Delta\mathbf{u} - \Delta\mathbf{u}^{vcr}) = \mathbf{E}(\Delta\mathbf{u} - \Delta\lambda\mathbf{A}\mathbf{n}) \tag{36}$$

$$\Delta q^{vcr} = \mathbf{t}^T \Delta\mathbf{u}^{vcr} \tag{37}$$

Thus, the viscoplastic consistency condition at iteration "i" can be expressed as a function of ${}^i\Delta(\lambda)$, ${}^i\overline{F}={}^i\overline{F}({}^i\Delta(\lambda))$. The viscoplastic consistency parameter ${}^i\Delta(\lambda)$ can be obtained similarly to classical inviscid elastoplasticity from the expression of a truncated Taylor's serie at the first term

$${}^i\overline{F}={}^{i-1}\overline{F}+{}^{i-1}\left(\frac{\mathrm{d}\overline{F}}{\mathrm{d}\Delta\lambda}\right){}^i\mathrm{d}\Delta\lambda = 0 \Rightarrow {}^i\mathrm{d}\Delta\lambda = -{}^{i-1}\overline{F}\left[{}^{i-1}\left(\frac{\mathrm{d}\overline{F}}{\mathrm{d}\Delta\lambda}\right)\right]^{-1} \tag{38}$$

As proposed by several authors, see a.o. Ponthot (1995), Wang (1997), Carosio et al. (2000), and to avoid further complication, it is supposed here that $\dot{\lambda}$ is accurately approximated by $\dot{\lambda} = \Delta\lambda/\Delta t$, i.e., $\Delta\lambda = \frac{\Delta t}{\eta}\langle\psi(F)\rangle$. This leads to $\mathrm{d}\dot{\lambda}/\mathrm{d}\Delta\lambda = 1/\Delta t$. Thus, the derivative of the viscoplastic yield function with respect to $\Delta\lambda$ takes the form

$$\frac{\mathrm{d}\overline{F}}{\mathrm{d}\Delta\lambda} = \mathbf{n}^T\frac{\mathrm{d}\mathbf{t}}{\mathrm{d}\Delta\lambda} + \left(\frac{\partial F}{\partial c}\frac{\mathrm{d}c}{\mathrm{d}q^{vcr}} + \frac{\partial F}{\partial\chi}\frac{\mathrm{d}\chi}{\mathrm{d}q^{vcr}}\right)\mathbf{t}^T\mathbf{m} - \frac{\eta}{\Delta t} \tag{39}$$

The change of the stresses with respect to $\Delta\lambda$ follows from Eq. (36) as

$$\frac{\mathrm{d}\mathbf{t}}{\mathrm{d}\Delta\lambda} = -\mathbf{E}^m\mathbf{m} \tag{40}$$

with

$$\mathbf{E}^m = \left[\mathbf{E}^{-1} + \Delta\lambda\frac{\partial\mathbf{m}}{\partial\boldsymbol{\sigma}}\right]^{-1} = (\mathbf{E}^{-1} + \Delta\lambda\mathbf{M})^{-1} \tag{41}$$

where $\mathbf{E}^m$ is the modified elastic matrix and $\mathbf{M} = \partial\mathbf{m}/\partial\mathbf{t}$ the hessian matrix for the interface model, which for a constant friction angle results:

- For $\sigma > 0$

$$\mathbf{M} = \begin{pmatrix} -2\tan^2\phi & 0 \\ 0 & 2 \end{pmatrix} \tag{42}$$

- For $\sigma < 0$

$$\mathbf{M} = \begin{pmatrix} -2f_c^{dil}\tan\phi\left[\frac{|\sigma|}{\sigma^{dil}}(c - \sigma\tan\phi) - \left(1 - \frac{|\sigma|}{\sigma^{dil}}\tan\phi\right)\right] & 0 \\ -2\left|\frac{\sigma\tan\phi}{\tau}\right|\tan\phi & 2\left|\frac{\sigma\tan\phi}{\tau}\right|\left[\frac{\sigma\tan\phi}{\tau} - 1\right] + 2 \end{pmatrix} \tag{43}$$

After replacing Eq. (40) in Eq. (39) and further in Eq. (38) we obtain the iteration formula for $\mathrm{d}\Delta\lambda$ as

$${}^i\mathrm{d}\Delta\lambda = -\frac{{}^{i-1}\overline{F}}{{}^{i-1}\left[-\mathbf{n}^T\mathbf{E}^m\mathbf{m} + \left(\frac{\partial F}{\partial c}\frac{\mathrm{d}c}{\mathrm{d}q^{vcr}} + \frac{\partial F}{\partial\chi}\frac{\mathrm{d}\chi}{\mathrm{d}q^{vcr}}\right)\mathbf{t}^T\mathbf{m} - \frac{\eta}{\Delta t}\right]} \tag{44}$$

from where the increment of the viscoplastic parameter ${}^i\Delta\lambda={}^{i-1}\Delta\lambda + {}^i\mathrm{d}\Delta\lambda$ is obtained and further those of the stress vector and state variable from Eqs. (36) and (37).

Please cite this article in press as: Lorefice, R. et al., Viscoplastic approach for rate-dependent failure analysis ..., Int. J. Solids Struct. (2008), doi:10.1016/j.ijsolstr.2007.12.016

5. Algorithmic tangent operator

In the framework of the finite element method, it is desirable to use an algorithmic tangent operator instead of the continuous one in order to preserve a quadratic convergence rate. The algorithmic tangent operator for the interface model can be formulated starting from the linearization of the viscoplastic consistency condition, see Eq. (14), for a finite increment “d”, quite similar to rate independent plasticity,

$$\mathrm{d}\overline{F} = \mathbf{n}^T \mathrm{d}\mathbf{t} + \bar{r}\mathrm{d}q - \eta \mathrm{d}\dot{\lambda} = 0 \tag{45}$$

The differential changes of the stress vector and state variables can be evaluated in a consistent form with the BE scheme

$$\mathrm{d}\mathbf{t} = \mathbf{E}^m(\mathrm{d}\mathbf{u} - \mathrm{d}\Delta\lambda\mathbf{m}) \tag{46}$$

$$\mathrm{d}q = \mathrm{d}\Delta\lambda\mathbf{t}^T\mathbf{A}\mathbf{n} + \Delta\lambda\mathrm{d}\mathbf{t}^T\mathbf{A}\mathbf{n} + \Delta\lambda\mathbf{t}^T\left(\frac{\mathrm{d}(\mathbf{A}\mathbf{n})}{\mathrm{d}\mathbf{t}}\right)\mathrm{d}\mathbf{t} \tag{47}$$

Substituting Eqs. (46) and (47) into Eq. (45) and after some algebra, we obtain

$$\mathrm{d}\Delta\lambda = \frac{\mathbf{n}^T\mathbf{E}^m\mathrm{d}\mathbf{u} + \beta\Delta\lambda\bar{r}}{\mathbf{n}^T\mathbf{E}^m\mathbf{m} - \alpha\bar{r} + \eta/\Delta t} \tag{48}$$

with the scalar values α, β defined as

$$\alpha = \mathbf{t}^T\mathbf{m} - \Delta\lambda\left(\mathbf{m}^T\mathbf{E}^m + \mathbf{t}^T\mathbf{M}\mathbf{E}^m\right)\mathbf{m} \tag{49}$$

$$\beta = \mathrm{d}\mathbf{u}^T\mathbf{E}^m\mathbf{m} + \mathbf{t}^T\mathbf{M}\mathbf{E}^m\mathbf{du} \tag{50}$$

Inserting Eq. (48) into the tangential stress–strain relation $\mathrm{d}\mathbf{t} = [\mathbf{E}^{alg}_{vp}]\mathrm{d}\mathbf{u}$, the algorithmic tangent operator for the continuum viscoplastic interface model is obtained as

$$[\mathbf{E}^{alg}_{vp}] = \left[\mathbf{E}^m - \frac{\mathbf{n}^T\mathbf{E}^m + \Delta\lambda\bar{r}[\mathbf{m}^T\mathbf{E}^m + \mathbf{t}^T\mathbf{M}\mathbf{E}^m]}{\mathbf{n}^T\mathbf{E}^m\mathbf{m} - \alpha\bar{r} + \eta/\Delta t}\right] \tag{51}$$

The numerical performance of this development is tested in the next section.

6. Numerical analysis

6.1. Efficiency assessment of stress integration procedure

We evaluate the numerical performance of the proposed rate-dependent interface model when three different approaches for the material operator are used: the consistent operator, the continuum operator and the continuum one with a subincrementation procedure by López Garello (1999). For this numerical performance evaluation the post-peak regime of the uniaxial tensile test is considered with decreasing number of displacement increments. The results are depicted in Fig. 2 whereby the”exact” solution that is obtained using very small displacement increments is indicated with solid line. The numerical tests were run using alternatively 6, 2, and 1 displacement increments. When 6 steps were considered, all the three numerical approaches leaded to very similar response behavior. However, the continuous operator procedure required significantly more iterations to achieve the convergence criterion than the continuum tangent with subincrementation, and, moreover, than the consistent tangent procedure. When up to 2 steps were considered the numerical schemes based on the consideration of continuum tangent without subincrementation techniques could not fulfill the convergence criterion. Contrarily, the convergence could be reached when the consistent tangent was used leading to an accurate solution of the algebraic problem. The convergence properties of the algorithms can further be investigated by looking at the residuum of the iteration procedure. Fig. 3 shows the evolution of the measured residuum norm versus the number of iteration steps obtained for one selected converged stress state of the numerical tests. In the analyses for Fig. 3 the non-linear branch is evaluated with 6, 2, and 1 steps (departing from a stress state at the beginning of the softening regime). In the same figure the convergence performance of the continuum tan-

Please cite this article in press as: Lorefice, R. et al., Viscoplastic approach for rate-dependent failure analysis ..., Int. J. Solids Struct. (2008), doi:10.1016/j.ijsolstr.2007.12.016

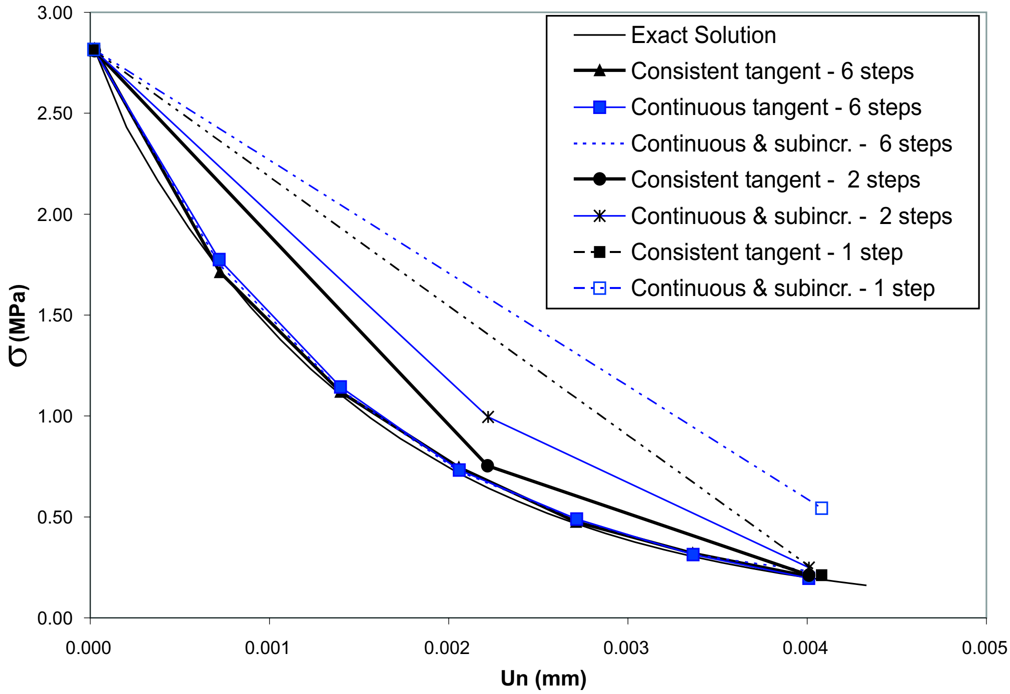

Fig. 2. Numerical efficiency – pure traction test.

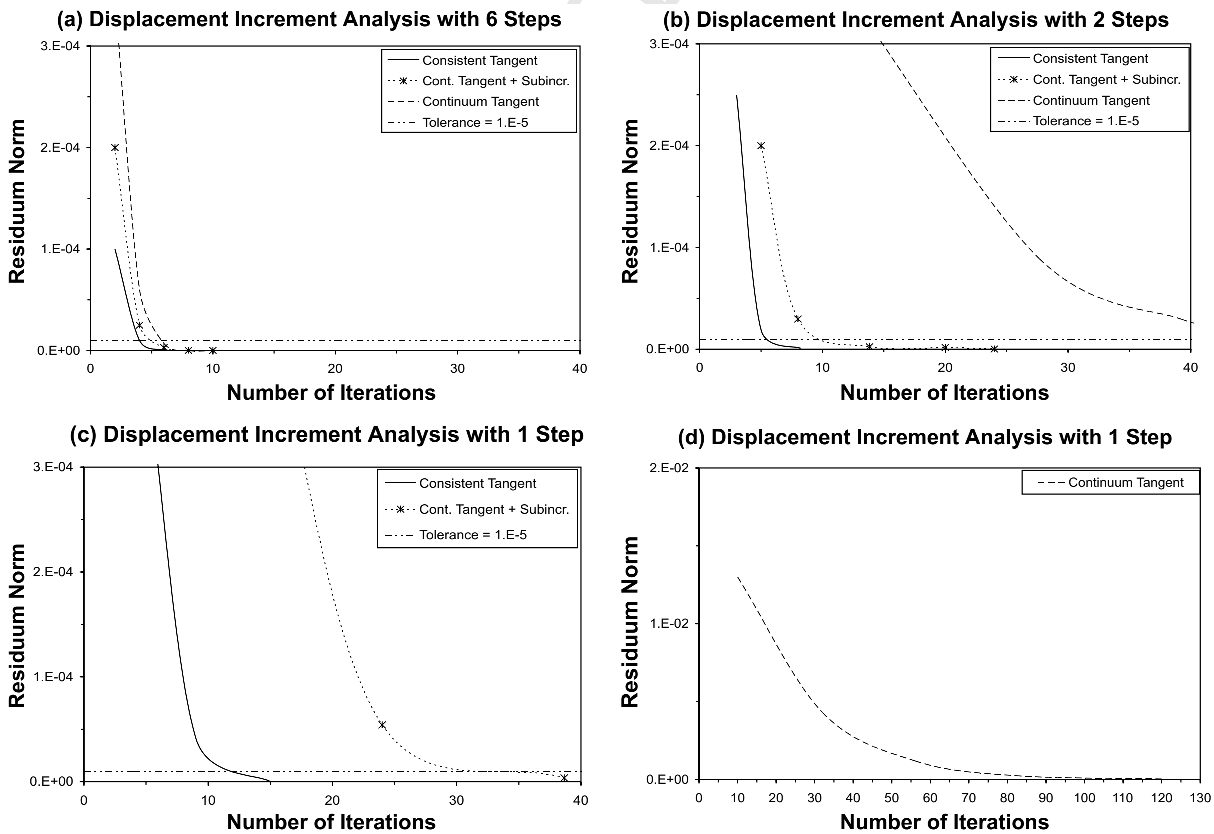

Fig. 3. Convergency behavior of compared algorithms.

gent shows that for 2 and 1 steps this algorithm fails to achieve the prescribed tolerance within the specified maximum number of iterations (50). The results in Figs. 2 and 3 demonstrate the superior numerical performance regarding robustness and efficiency of the algorithmic or consistent tangent operator for the proposed time-dependent interface model.

6.2. Model calibration

In the framework of the viscoplastic flow theory the time dependence of the material parameters and particularly the over-strength is introduced by the viscosity η. To properly reproduce the complex variation of the concrete tensile over-strength with the applied loading rate, a velocity-dependent description of the viscosity parameter needs to be incorporated. In this work, and based on the considered calibration tests by Suaris and Shah (1984, 1985), the following evolution law for the viscosity is proposed in terms of the applied velocity

$$\eta = \eta(\dot{u}) = \eta_0[\alpha \ln(\dot{u}) + \beta\sqrt{\dot{u}} + \gamma] \tag{52}$$

whereby $\dot{u}$ represents the displacement rate at the interface, and the coefficients are $\alpha = 0.072$, $\beta = 0.719$ and $\gamma = 1.678$, while the initial viscosity is $\eta_0 = 1.E5$ MPa.sec. The prediction of the interface model in terms of the tensile dynamic increase factor DIF is plotted in Fig. 4 and compared versus experimental results. The stress-displacement response for different velocities are shown in Fig. 5 and compared versus experimental results. The numerical analyses were carried-out in a range of velocities between 1.0E-6 and 1.0 mm/s. For the purpose of verification of the present model, stresses and displacements reported in the experiments were considered as average values at the interface. Model parameters were set as: $E_N = 30000$ MPa/mm, $\chi_0 = 5.37$ MPa, $G_f^I = 0.03$ N/mm, $G_f^{II} = 10G_f^I$, and shape coefficients $\alpha_\chi = \alpha_c = 0$. Model predictions are in good agreement with the measured peak values, but unfortunately, experimental results of the dynamic response of concrete specimens are not available for the softening branch, so model predictions after that point cannot be tested. The results also demonstrate, that in one extreme case when $\eta/\Delta t \to 0$, as expected, the viscoplastic model leads to the same prediction of the inviscid elastoplastic formulation while in the other extreme case when $\eta/\Delta t \to \infty$ the elastic solution is approximated.

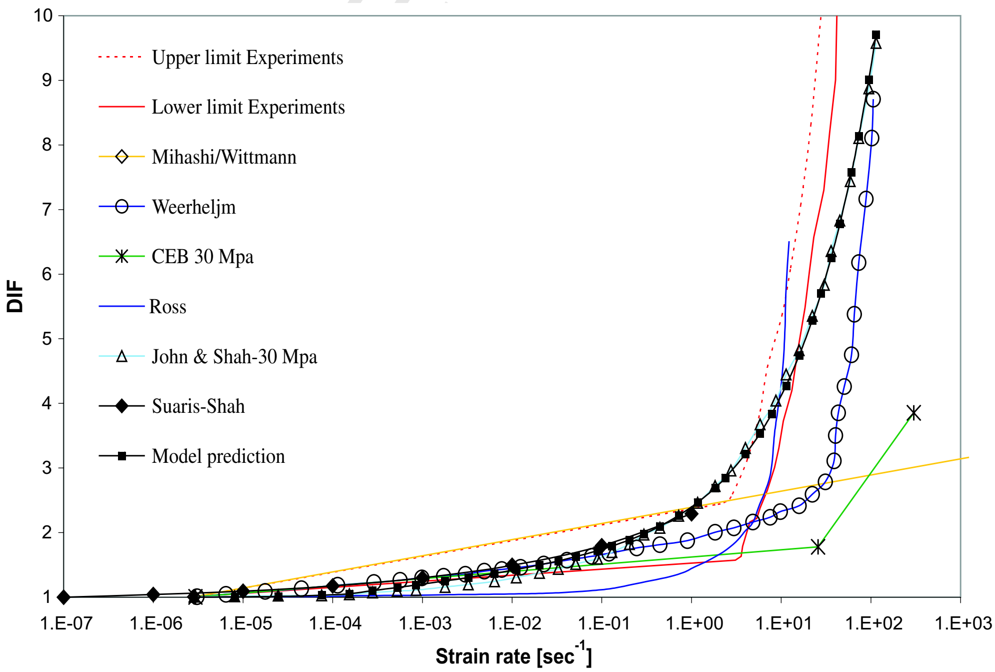

Fig. 4. Dynamic increase factor in the uniaxial tensile tests.

Please cite this article in press as: Lorefice, R. et al., Viscoplastic approach for rate-dependent failure analysis ..., Int. J. Solids Struct. (2008), doi:10.1016/j.ijsolstr.2007.12.016

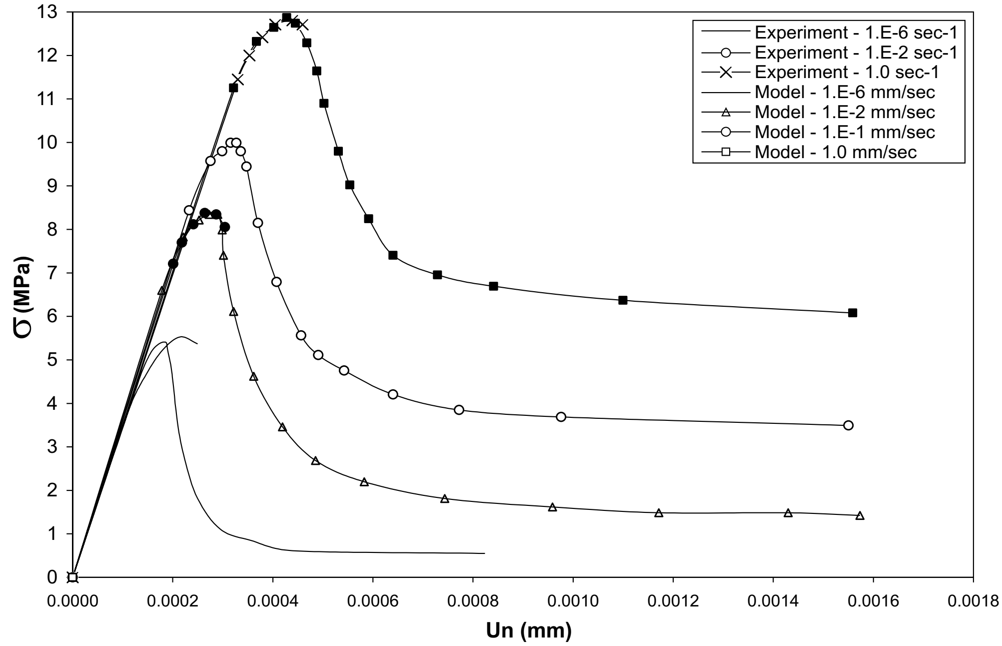

Fig. 5. Pure tension test – constitutive response.

6.3. Prediction of sudden changes of the loading rate

Experimental evidence indicates that the mechanical response of quasi-brittle materials like rock, concrete or ceramics are sensitive to changes in the applied loading rate. This effect has been recently investigated by several authors, see among others Bažant et al. (1993, 1995), Tandon et al. (1995), Bažant and Gettu (1992). The work by Tandon et al. (1995) that includes a comprehensive experimental study on normal and high strength concrete specimens of different sizes using the three point bending test on notched beams demonstrates that for a large increase of the applied loading rate or velocity, the post-peak softening may reverse to hardening followed by a second peak of the stress-strain or stress-displacement curves. In the case of a sudden decrease of the velocity, a steeper slope is obtained for the softening branch, either for normal or high strength concrete quality. In this section, the interface model capability to capture the reversal of softening effect is studied starting from the previously presented computational simulations of the tensile tests at several displacement rates. To this end, a sudden change of the applied velocity (decrease or increase) is considered from the so-called *restart points* located on the softening branch of the different tensile response curves, see Fig. 6. For a sudden velocity increase, the softening response turns into hardening behavior, with a second stress peak. The numerical response stabilizes reaching the corresponding applied velocity slope to the higher velocity. In the same figure, after a sudden decrease of loading rate, the slope of the stress-displacement diagram becomes steeper, following a softening response that evolves until reaching the softening curve corresponding to the lower velocity. It can be noted that immediately after velocity reduction, the experimentally observed stress relaxation effect is captured. The numerical tests in this section indicates that the proposed model is capable to qualitatively reproduce the global observed experimental behavior regarding reverse of softening effects due to sudden velocity changes.

6.4. Shear/compression tests

A second set of numerical simulations was performed to investigate the predictive capabilities of the visco-plastic model under shear/compression stress states at different strain rates. In the first set of tests, an initial load step is applied to impose a compressive stress state over the interface. Then, the shear relative displace-

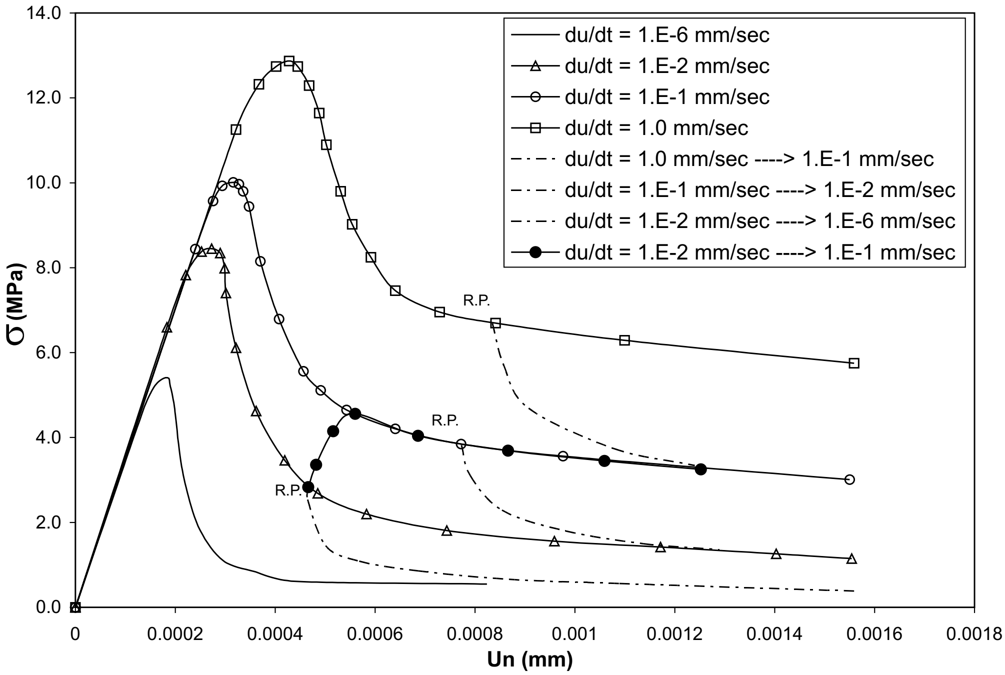

Fig. 6. Reversal of softening effect – constitutive response.

ment in the joint is progressively increased while keeping the compression constant. Fig. 7 shows the constitutive response in terms of shear stress versus relative tangential displacement for compressive stresses of 2.0

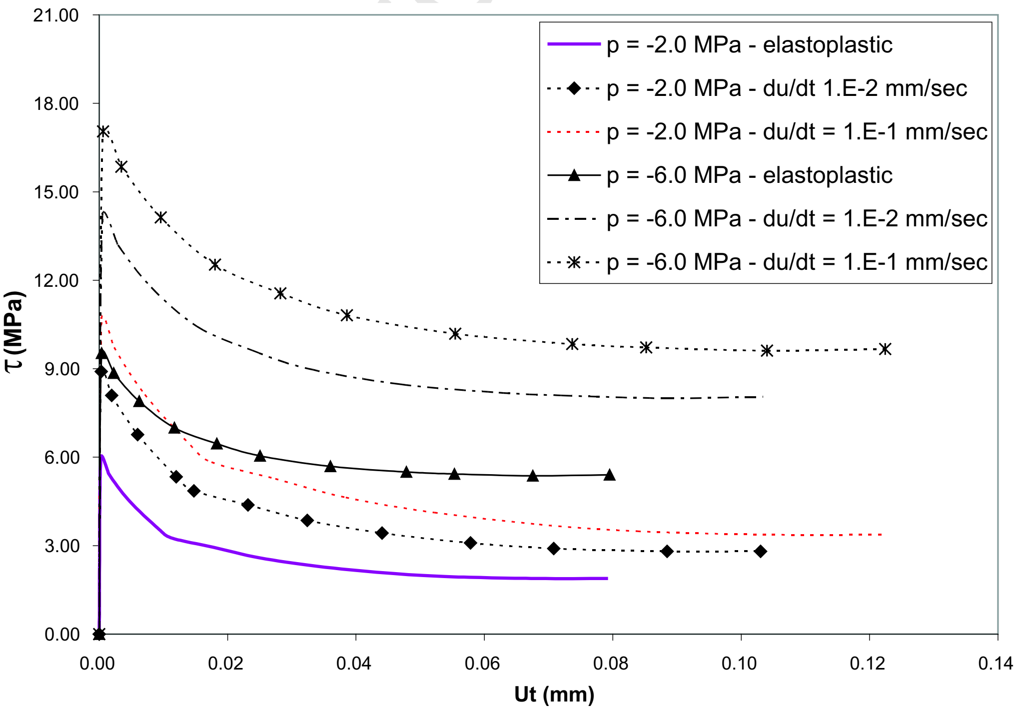

Fig. 7. Shear test under different compressive states.

and 6.0 MPa. The family of curves shows that an increasing shear strength are obtained for higher confinement pressures as well as for higher relative displacement rates. An additional effect of the velocity increment is the higher ductility of the post-peak branches as well as the related energy release. Unfortunately, no experimental evidence was found to verify this effect of the velocity increase on the fracture mechanics properties of concrete and/or mortar. The evolution of dilatancy is represented in the form of normal relative displacement against shear relative displacement and plotted in Fig. 8. In case of the rate-independent model formulation the increase of the dilatancy in the normal direction to the joint takes place for decreasing confining pressures. However, in case of the rate-dependent model an additional increase of normal dilatancy is obtained for increasing velocities.

Figs. 9–14 show model performance when compared against the experimental results by Hassanzadeh (1992). These tests consisted on imposing combined normal and shear relative displacements to a developing crack in a prismatic concrete specimen of $0.07 \times 0.07\ \mathrm{m}^2$ square cross section with a perimeteral 0.015 m deep notch. During the first part of the numerical tests, a uniaxial tensile stress was imposed until the peak strength is reached. From that stress state, a fixed ratio $\theta = u_n/u_t$ was applied, with u_n and u_t the normal and tangential relative displacements, respectively. All these experiments were carried-out under monotonically increasing displacement control at the crack mouth in order to ensure stable crack propagation. The Hassanzadeh tests were also considered by other authors to calibrate and/or validate the predictions of material models at constitutive levels of observations, see Ali (1996), Carol et al. (1997), Cocchetti et al. (2002), Parland and Miettinen (2002), López Garello (1999). In this sense, for continuum type of material models the Hassanzadeh tests were considered at the global stress-strain level, while for discrete models like the present one these tests are considered at the stress-relative displacement level. In both cases homogeneous distribution of the global strains and of the relative displacements at the crack mouth are assumed. In this work tests were run with $\theta = 30°$ and $\theta = 60°$. The model parameters value used in these numerical analysis are: $E_N = E_T = 200$ MPa/m, $tan\phi = 0.9$, $\chi_0 = 2.8$, $c_0 = 7$ MPa, $G_f^I = 0.1$ N/mm, $G_f^{II} = 10G_f^I$, $\sigma_{dil} = 56$ MPa, $\alpha_x = 0$, $\alpha_c = 1.5$. The results in Fig. 9 show that the tangential and normal displacement control in the second part of the Hassanzadeh test for $\theta = 30°$ is responsible for a stronger softening of the normal tensile stress than

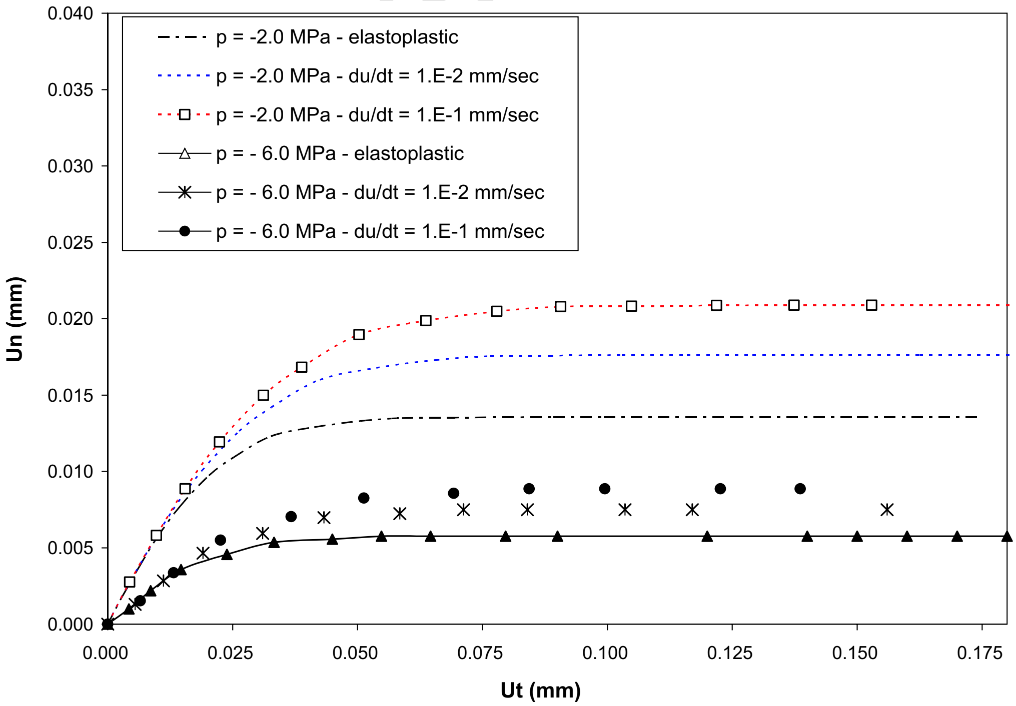

Fig. 8. Dilatancy evolution – confined shear test.

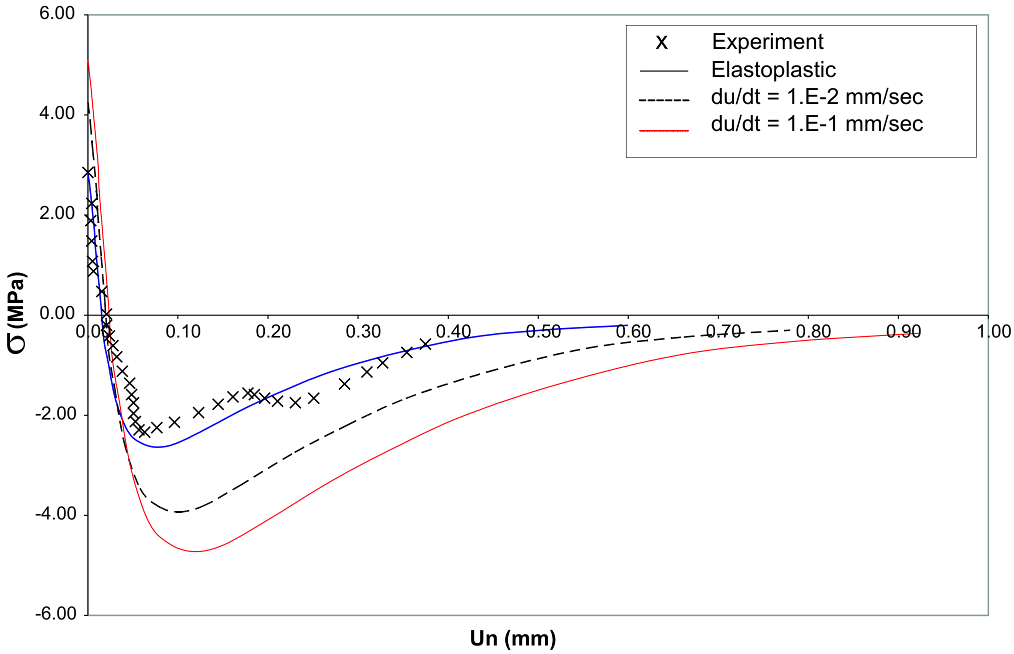

Fig. 9. Hassanzadeh test – normal stress vs. normal relative displacement for $\theta = 30°$.

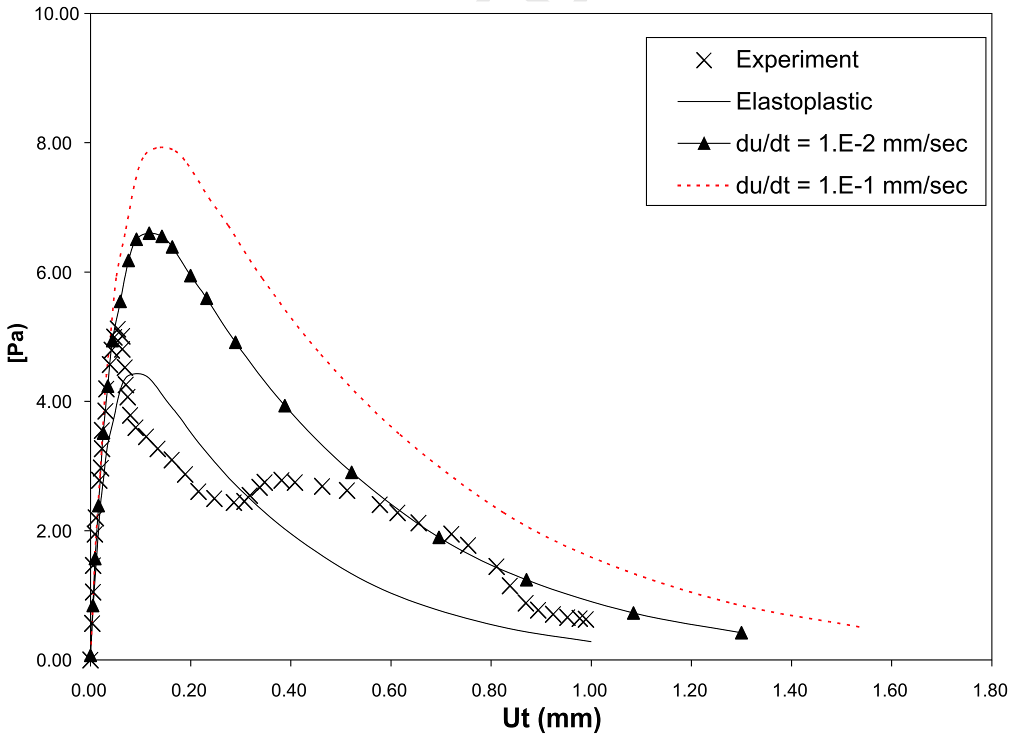

Fig. 10. Hassanzadeh test – shear stress vs. tangential relative displacement for $\theta = 30°$.

in case of the pure tension test. After the tensile normal stress reduces to zero compressive normal stress develops up to a peak value from where a final softening branch (in compression) follows. This behavior as well as

Please cite this article in press as: Lorefice, R. et al., Viscoplastic approach for rate-dependent failure analysis ..., Int. J. Solids Struct. (2008), doi:10.1016/j.ijsolstr.2007.12.016

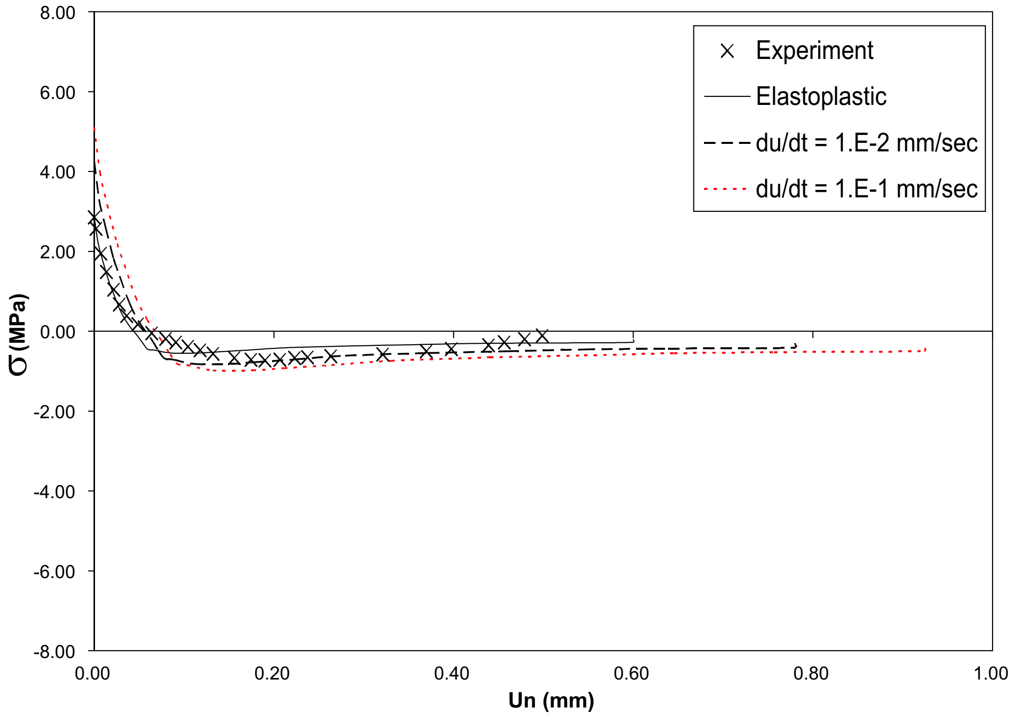

Fig. 11. Hassanzadeh test – normal stress vs. normal relative displacement for $\theta = 60°$.

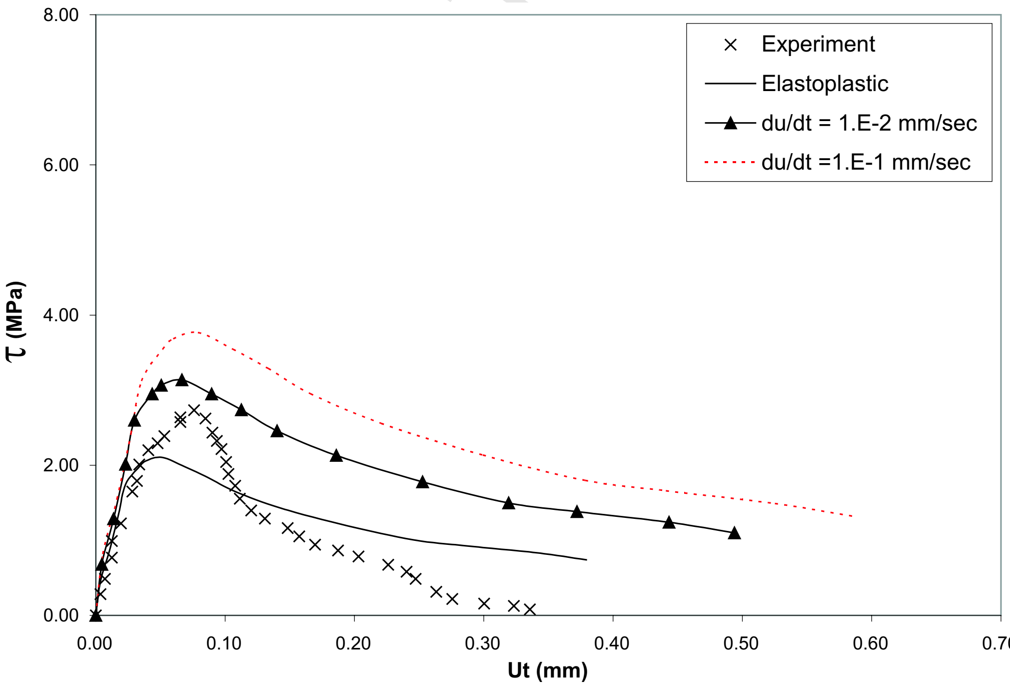

Fig. 12. Hassanzadeh test – shear stress vs. tangential relative displacement for $\theta = 60°$.

449 the peak normal stresses in tensile and compressive regimes are less significant in case of the $\theta = 60°$ in Has-
450 sanzadeh's test, as can be observed in Fig. 11. It is important to note, that the increment of velocity in both

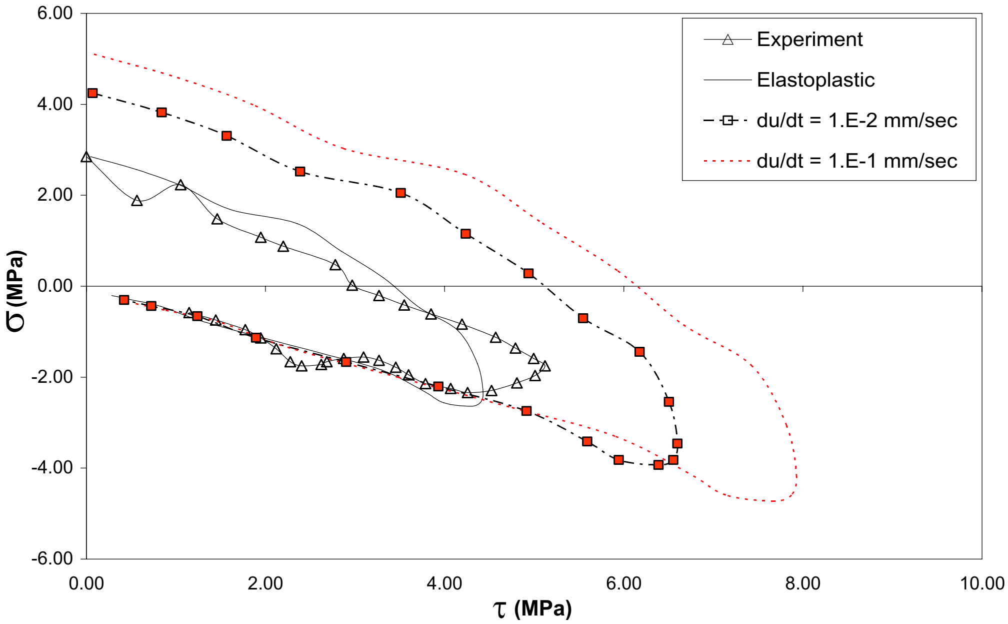

Fig. 13. Hassanzadeh test – normal stress vs. shear stress $\theta = 30°$.

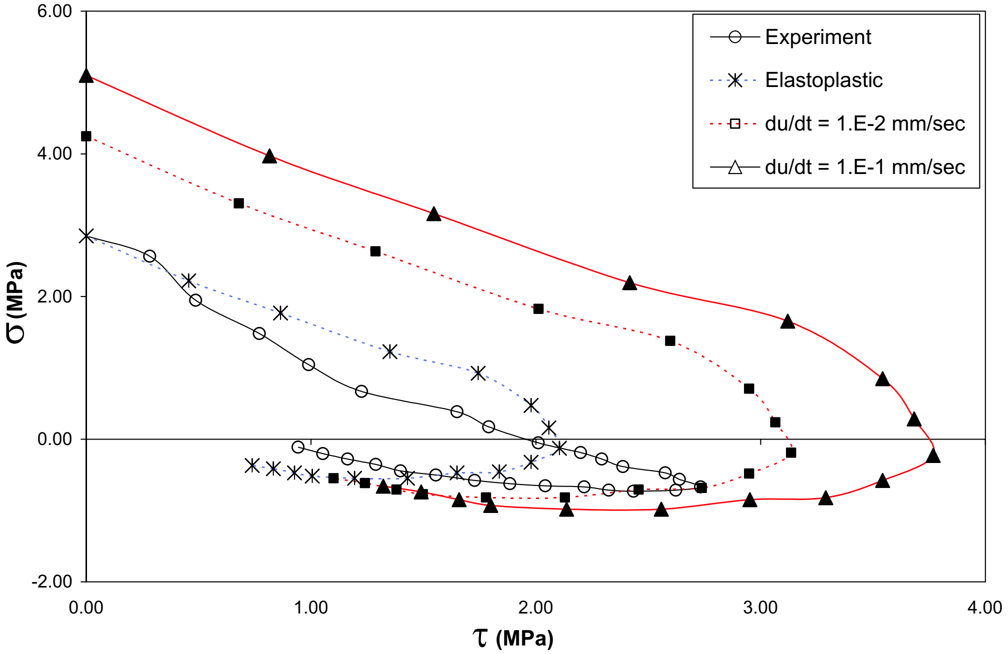

Fig. 14. Hassanzadeh test – normal stress vs. shear stress $\theta = 60°$.

tests leads to an increase of the peak normal stresses together with a more ductile behavior in the post peak regime.

Regarding the behavior of the shear stress in terms of the tangential relative displacement in Figs. 10 and 12, similar conclusions to those corresponding to the performance of the normal stress related to the normal relative displacement can be obtained. In other words, a reduction of the peak shear stress and an increment of the ductility can be obtained by increasing the value of θ or by decreasing the applied velocity. Finally, Figs. 13 and 14 plot the evolution of normal stresses against shear stresses during those tests.

7. Conclusions

A new rate-dependent viscoplastic interface model for quasi-brittle materials like concrete and mortar was presented. The proposed model is based on the inviscid elastoplastic interface formulation by Carol et al. (1997) and on the continuous Perzyna's theory for time-dependent material behavior. For the stress integration procedure during finite viscoplastic processes an extension of the well known Closest Point Projection Method for rate-independent elastoplasticity was developed. To assure quadratic rate of convergence in finite element analysis of deformation problems of quasi-brittle materials with the proposed rate-dependent interface model the algorithmic or consistent tangent operator was formulated from the linearized form of the generalized consistency condition. The proposed model parameters were calibrated with the experimental results by Suaris and Shah (1984, 1985) of uniaxial tensile tests on concrete specimens at different strain rates. To capture the non-linear variation of the tensile strength of concrete with the applied strain rate, an internal logarithmic function of the interface viscosity in terms of the velocity is proposed that was calibrated with the above indicated experimental tests. The computational results in this paper demonstrate the capability of the proposed rate-dependent interface model to reproduce the most relevant features of brittle material dynamic failure. In this sense, the numerical predictions fits very well the overstrength of concrete under increasing velocity as well as the reversal of softening effects by sudden velocity changes. The model is also able to capture the interaction between the rate effects and the time effects that develop in mortar and concrete for strain rates in the range of 1.0E-6 to 1.0E-4 s^{-1}. The proposed rate-dependent interface model is a suitable numerical tool for discrete analysis of transient failure processes in quasi-brittle materials at the mesostructural level of observation.

Acknowledgements

The first author acknowledges the partial support of this research by the *Universidad de Santiago del Estero*. The second author wants to acknowledge the partial support of this research by the *Universidad de Buenos Aires* and by the Argentina Agency for the Promotion of Research and Technology.

References

Ali, A., 1996. FEM analysis of concrete structures subjected to Mode-I and mixed-mode loading conditions. Computers and Structures 61 (6), 1043–1055.
Antoun, T.H., 1991. Constitutive/failure model for the static and dynamic behaviors of concrete incorporating effects of damage and anisotropy. Ph.D. Thesis, University of Dayton, Dayton, Ohio.
Bažant, Z.P., Oh, B.H., 1982. Strain-rate effect in rapid triaxial loading of concrete. Journal of Engineering Mechanics Division, ASCE 108 (5), 764–782.
Bažant, Z.P., Gettu, R., 1992. Rate effects and load relaxation in static fracture of concrete. ACI Materials Journal 89 (5), 456–468.
Bažant, Z.P., Bai, S.P., Gettu, R., 1993. Fracture of rock: effect of loading rate. Engineering Fracture Mechanics (45), 393–398.
Bažant, Z.P., Gu, W.H., Faber, K.T., 1995. Softening reversal and other effects of a change in loading rate on fracture of concrete. ACI Materials Journal (92), 3–9.
Bažant, Z.P., Li, Y.N., 1997. Cohesive crack with rate-dependent opening and viscoelasticity. I: mathematical model and scaling. International Journal of Fracture 86 (3), 247–265.
Bažant, Z.P., Caner, F.C., Adley, M.D., Akers, S.A., 2000. Fracturing rate effect and creep in microplane model for dynamics. Journal of Engineering Mechanics 126 (9), 962–970.
Brara, A., Klepaczko, J.R., 2006. Experimental characterization of concrete in dynamic tension. Mechanics of Materials 38, 253–267.
Birkimer, D.L., 1968. Critical normal fracture strain of portland cement concrete. Ph.D. thesis, University of Cincinnati.
Birkimer, D.L., Lindemann, R., 1971. Dynamic tensile strength of concrete materials. ACI Journal, Proceedings, 47–49.
Bresler, B., Bertero, W., 1975. Influence of high strain rate and cyclic loading of unconfined and confined concrete in compression. In: Proceedings of Second Canadian Conference On Earthquake Engineering, pp. 1–13.
Burlion, N., Gatuingt, F., Pijaudier-Cabot, G., Daudeville, L., 2000. Compaction and tensile damage in concrete: constitutive modelling and application to dynamics. Computer Methods in Applied Mechanics and Engineering 183, 291308.

Please cite this article in press as: Lorefice, R. et al., Viscoplastic approach for rate-dependent failure analysis ..., Int. J. Solids Struct. (2008), doi:10.1016/j.ijsolstr.2007.12.016

Cadoni, E., Albertini, C., Labibes, K., Solomos, G., 2001a. Behavior of plain concrete subjected to tensile loading at high strain rate. In: de Borst et al. (Eds.), Fracture Mechanics of Concrete Structures. Swets and Zeitlinger, Lisse, pp. 341–347.

Cadoni, E., Labibes, K., Albertini, C., Berra, M., Giangrasso, M., 2001b. Strain rate effect on the tensile behaviour of concrete at different relative humidity levels. Materials and Structures 34, 21–26.

Carol, I., Prat, P.C., López, C.M., 1997. Normal/shear cracking model. Interface implementation for discrete analysis. Journal of Engineering Mechanics, ASCE 123 (8), 765–773.

Carosio, A., Willam, K., Etse, G., 2000. On the consistency of viscoplastic formulations. Interantional Journal of Solids and Structures (37), 7349–7369.

Chang, C.S., Wang, T.K., Sluys, L.J., Van Mier, J.G.M., 2002a. Fracture modelling with a microstructural mechanics approach - 1. Theory and formulation. Engineering Fracture Mechanics 17 (69), 1941–1958.

Chang, C.S., Wang, T.K., Sluys, L.J., Van Mier, J.G.M., 2002b. Fracture modelling with a microstructural mechanics approach - 2. Finite element analysis. Engineering Fracture Mechanics 17 (69), 1959–1976.

Cocchetti, G., Maier, G., Shen, X.P., 2002. Linear models for interfaces and mixed mode cohesive cracks. CMES – Computer Modeling in Engineering and Sciences 3 (3), 279–298.

Cowell, W.L., 1966. Dynamic properties of plain portland cement concrete. Technical Report R447, Naval Civil Engineering Laboratory, Port Hueneme, CA.

Dhir, R.K., Sangha, C.M., 1972. Study of the relationships between time, strength, deformation and fracture of plain concrete. Magazine of Concrete Research 24 (81), 197–208.

Dilger, W.H., Koch, R., Kowalczyk, R., 1978. Ductility of Plain and Confined Concrete Under Different Strain Rates. American Concrete Institute, Spec. Pub., Detroit, Michigan, pp. 121–135.

Etse, G., Carosio, A., 2002. Diffuse and localized failure predictions of Perzyna viscoplastic models for cohesive – frictional materials. Latin American Applied Research (32), 21–31.

Grote, D.L., Park, S.W., Zhou, M., 2001. Behavior of concrete at high strain rates and pressures: I. Experimental characterization. Interantional Journal of Impact Engineering 25, 869–886.

Hassanzadeh, M., 1992. Behavior of fracture process zone in concrete influenced by simultaneously applied normal and shear displacements. PhD. Thesis, Lund Institute of Technology, Lund, Sweden.

Hatano, T., Tsutsumi, H., 1960. Dynamical compressive deformation and failure of concrete under earthquake load. In: Proceedings of Second World Conference on Earthquake Engineering. Tokyo Science Council of Japan, pp. 1963–1978.

Hughes, B.P., Gregory, R., 1972. Concrete subjected to high rates of loading in compression. Magazine of Concrete Research 24 (78), 25–36.

Hughes, B.P., Watson, A.J., 1978. Strength and ultimate strain of concrete under impact loading. Magazine of Concrete Research 30 (105), 189–199.

John, R., Shah, S.P., 1987. Effect of high strength and rate of loading on fracture parameters of concrete. In: Shah, S.P., Swartz, S.E. (Eds.), SEM/RILEM Conference on Fracture of Concrete and Rock, Houston, Texas, pp. 35–52.

John, R., Antoun, T., Rajendran, A.M., 1992. Effect of strain rate and size on tensile strength of concrete. In: Schmidt, S.C., Dick, R.D., Forbes, J.W., Tasker, D.G. (Eds.), Proceedings, APS Topical Conference on Shock Compression of Condensed Matter. Elsevier Science Publishers, Williamsburg, VA, pp. 501–504.

Kormeling, H.A., Zielinski, A.J., Reinhardt, H.W., 1980. Experiments on concrete under single and repeated uniaxial impact tensile loading. Stevin Report 5-80-3, Delft University of Technology.

Li, Y.N., Bažant, Z.P., 1997. Cohesive crack with rate-dependent opening and viscoelasticity. II: numerical algorithm, behavior and size effect. Interantional Journal of Fracture 86 (3), 267–288.

López Garello, C.M., 1999. Análisis Microestructural de la Fractura del Hormigón Utilizando Elementos Tipo Junta. Aplicación a Diferentes Hormigones. PhD. Thesis, Universitat Politécnica de Catalunya, Barcelona, Spain (in spanish).

Malvern, L.E., Tang, T., Jenkins D.A., Gong, J.C., 1985. Dynamic compressive strength of cementitious materials. Symposium Material Research Society.

McVay, M.K., 1988. Spall damage of concrete structures. Technical Report SL-88-22, U.S. Army Corps of Engineers. Waterways Experiment Station, Vicksburg, MS.

Parland, H., Miettinen, A., 2002. On the stiffness characteristics of nonmonolithic elastic structures. Part I. Theory. International Journal of Solids and Structures 39 (6), 1673–1699.

Park, S.W., Xia, Q., Zhou, M., 2001. Dynamic behavior of concrete at high strain rates and pressures: II. Numerical simulation. Interantional Journal of Impact Engineering 25, 887–910.

Perzyna, P., 1966. Problems in viscoplasticity. Advances in Applied Mechanics 9, 244–368.

Ponthot, J.P., 1995. Radial return extensions for viscoplasticity and lubricated friction. In: Proceedings of International Conference on Structural Mechanics and Reactor Technology SMIRT-13, Porto Alegre, Brazil, (2), pp. 711–722.

Reinhardt, H.W., 1982. Under impact loading – tensile strength and bond. HERON 3 (27).

Reinhardt, H.W., 1984. Tensile fracture of concrete at high rates of loading. In: Shah, S.P. (Ed.), Application of Fracture Mechanics to Cementitious Composites, NATO-ARW, pp. 559–590.

Reinhardt, H.W., 1985. Strain rate effects on the tensile strength of concrete as predicted by thermodynamics and fracture mechanics models. In: Mindess, S., Shah, S.P. (Eds.), Cement Based Composites: Strain Rate Effects on Fracture, pp. 1–13.

Ross, C.A., Thompson, P.Y., Tedesco, J.W., 1989. Split-hopkinson pressure-bar tests on concrete and mortar in tension and compression. ACI Materials Journal 5 (86), 475–481.

Ross, C.A., 1991. Fracture of concrete at high strain rate. Proceedings NATO Advanced Research Workshop: Toughening Mechanism in Quasi-Brittle Materials, Northwestern University, Evanston, Illinois. Kluwer Academic Publishers., The Netherlands, pp. 577–591.

Ross, C.A., Tedesco, J.W., Kuennen, T.S., 1995. Effects of strain rate on concrete strength. ACI Materials Journal 1 (92), 37–47.
Ross, C.A., Jerome, D.M., Tedesco, J.W., Hughes, M.L., 1996. Moisture and strain rate effects on concrete strength. ACI Materials Journal 3 (94), 293–300.
Rossi, P., van Mier, J.G.M., Boulay, C., le Maou, F., 1992. The dynamic behaviour of concrete: influence of free water. Materials and Structures 25, 509–514.
Rossi, P., 1997. Strain rate effects in concrete structures: the lcpc experience. Materials and Structures Supplement March, pp. 54–62.
Ruiz, G., Ortiz, M., Pandolfi, A., 2000. Three dimensional finite-element simulation of the dynamic Brazilian tests on concrete cylinders. International Journal for Numerical Methods in Engineering 48 (7), 963–994.
Shi, C., van Dam, A.G., Sluys, L.J., Van Mier, J.G.M., 1999. Crack interaction in concrete, In: Conference in Proceedings of EUROMAT 99.
Slowik, V., Leite, J.P., 2000. Meso-level modelling of concrete fracture. LACER N5.
Sluys, L.J., Liu, W.Y., 2003. Meso-level analysis to the behavior of concrete under impact loading. In: Oñate, E., Owen, D.R.J. (Eds.), Proceedings of Seventh International Conference on Computational Plasticity (COMPLAS VII), Barcelona, Spain, in CDROM.
Stankowski, T., 1990. Numerical simulation of progressive failure in particle composites. PhD Thesis, University of Colorado, Boulder, Colorado, USA.
Suaris, W., Shah, S., 1984. Rate-sensitive damage theory for brittle solids. Journal of Engineering Mechanics, ASCE 6 (110), 985–997.
Suaris, W., Shah, S., 1985. A constitutive model for concrete under dynamic loading. Journal of Structural Engineering, ASCE 111 (3), 563–576.
Takeda, J.J., Tachikawa, H., 1962. Mechanical properties of several kinds of concrete at compressive, tensile and flexural tests in high rates of loading. Transactions of Architect Institute Japan 77, 1–6.
Takeda, J.J., Tachikawa, H., 1971. Deformation and fracture of concrete subjected to dynamic load. Mechanical behavior of materials, In: Proceedings of the International Conference, Kyoto, (IV).
Tandon, S., Faber, K.T., Bažant, Z.P., Li, Y.N., 1995. Cohesive crack modelling of influence of sudden changes in loading rate on concrete fracture. Engineering Fracture Mechanics 52 (6), 987–997.
Tedesco, J.W., Ross, C.A., Brunair, R.M., 1989. Numerical analysis of dynamic split cylinder tests. Computers and Structures 3/4 (32), 609–624.
Tedesco, J.W., Ross, C.A., McGill, P.B., O'Neil, B.P., 1991. Numerical analysis of high strain rate concrete direct tension tests. Computers and Structures 2 (40), 313–327.
Tedesco, J.W., Ross, C.A., Kuennen, S.T., 1993. Experimental and numerical analysis of high strain rate splitting tensile tests. ACI Materials Journal 2 (90), 162–169.
Tedesco, J.W., Powell, J.C., Ross, C.A., Hughes, M.L., 1997. A strain rate dependent concrete material model for ADINA. Computers and Structures 4/5 (64).
Tvergaard, V., Hutchinson, J.W., 1993. The influence of plasticity on mixed-mode interface toughness. Journal of the Mechanics and Physics of Solids 41, 1119–1135.
Vervuurt, A., 1997. Interface fracture in concrete. PhD. dissertation. Delft University of Technology, The Netherland.
Vonk, R., 1992. Softening of concrete loaded in compression. PhD. dissertation. Technische Universiteit Eindhoven, Eindhoven, The Netherland.
Wang, W.M., 1997. Stationary and propagative instabilities in metals – a computational point of view. PhD Thesis. TU-Delft. The Netherlands.
Wang, W.M., Sluys, L.J., 2000. Formulation of an implicit algorithm for finite deformation viscoplasticity. International Journal of Solids and Structures 37 (48), 7329–7348.
Wang, T.K., Bittencourt, T.N., 2001. Simulation of crack propagation in concrete using a lattice model for the mesostructure, In: Conference in Proceedings of XXII CILAMCE, Campinhas, Brazil.
Watstein, D., 1953. Effect of straining rate on the compressive strength and elastic properties of concrete. Journal of American Concrete Institute (49), 719–729.
Weerheijm, J., Doormaal, J.C.A.M., van de Kasteele, R.M., 2001. Development of a new test set-up for dynamic tensile tests on concrete under high loading rates. Part 1: results of test series A. Rijswijk:TNO.
Weerheijm, J., Doormaal, J.C.A.M. van de Kasteele, R.M., 2003. Development of a new test set-up for dynamic tensile tests on concrete under high loading rates. Part 2: results and evaluation of test series B and C on concrete. Rijswijk:TNO.
Winnicki, A., Pearce, C.J., Bićanić, N., 2001. Viscoplastic Hoffman consistency model for concrete. Computers and Structures 79, 7–19.
Xu, X.P., Needleman, A., 1994. Numerical simulations of fast crack growth in brittle solids. Journal of the Mechanics and Physics of Solids 42, 1397–1434.

Please cite this article in press as: Lorefice, R. et al., Viscoplastic approach for rate-dependent failure analysis ..., Int. J. Solids Struct. (2008), doi:10.1016/j.ijsolstr.2007.12.016